Journal of Engineering Mechanics and Machinery (2023)
Clausius Scientific Press, Canada

DOI: 10.23977/jemm.2023.080303
ISSN 2371-9133 Vol. 8 Num. 3

Improved Blade Element Theory and Autorotating Rotor Aerodynamic Characteristics Analysis

Jizhen Li[1], Bing Lan[2]

[1]*School of Mechanical Engineering, Southeast University, Nanjing, 210000, Jiangsu, China*
[2]*Nanjing Research Institute of Simulation Technology, Nanjing, 210000, Jiangsu, China*

Keywords: Autorotating rotor; fixed wake; the Blade Element Theory; induced velocity; circulation

Abstract: During forward flight, the flow field of autorotating rotor was very complicated, which caused induced velocity of the disc plane difficult to be obtained. In order to analyze aerodynamic characteristics of the autorotating rotor, improved blade element theory, using the unlimited-bladed fixed wake method to establish a mathematical model, which could obtain velocity of the disc plane induced by fixed wake of autorotating rotor. According to the Biot-Savert Theorem, the expression of axial induced velocity of disc plane could be got by integerating. The circulation and induced velocity were all expanded into Fourier series by azimuth, and then axial induced velocity could be carried out by iteration. Combined the blade element theory, aerodynamic forces of the autorotating rotor was obtained, and then analyzed its aerodynamic characteristics.

1. Introduction

Rotor autorotation is a regular operating state of an autogyro in a steady flight; and aerodynamic characteristics of the autorotating rotor are the basis for studying flight performance of the autogyro[1]. Considering that flow field variations of the rotor in a forward flight mode are dramatically complex, no appropriate induced velocity distribution in the corresponding disc can be achieved by a traditional momentum or blade element theory. Consequently, some errors may be incurred during analyses on the aerodynamic characteristics of the autorotating rotor. Although the vortex theory can figure out rather proper induced velocity distribution by analyzing the rotor wake, it still fails to more profoundly probe into distributions of incidence and lift, etc. in the disc. In addition, rather realistic rotor flow fields can be simulated by numerical calculations, which is beneficial for in-depth studies on details of the flow field, such as interference and distortion of the vortex system; however, it is difficult to achieve convergence in the solving process on one hand and of a high computational complexity, so that such a method is inconvenient for engineering applications.

This paper was intended to establish a mathematical model for the induced velocity, generated by the fixed vortex system of the autorotating rotator in a forward flight, at a point in the disc based on the improved blade element theory and a fixed wake approach. According to the blade element theory, the Kutta-Joukowski theorem and the motion equation of flapping[2], a relationship was designed for circular rector and the induced velocity on one hand; and on the other hand, induced

velocity distribution was clarified in the disc. Besides, aerodynamic force of the rotor was also worked out by means of the blade element theory, so as to analyze its aerodynamic characteristics. In terms of the fixed wake approach, it can be adopted to identify an appropriate induced velocity distribution in the disc. After that, distributions of incidence and lift, etc. in the disc were further analyzed with the help of the blade element theory. In a word, the proposed method is suitable for calculating and analyzing rotors' aerodynamic characteristics in the engineering field.

2. Improvements of the blade element theory

By improving the blade element theory, the fixed wake approach was utilized to determine the induced velocity distribution in a disc, and further clarify both the relative airflow and the element force for the blade element. Through integration, the aerodynamic force of the autorotating rotor was achieved later.

To calculate the induced velocity of a single vortex cylinder relative to a point in the disc, a slant spiral vortex surface was divided into two parts of circular and straight vortex cylinders[3], as shown in Figure 1.

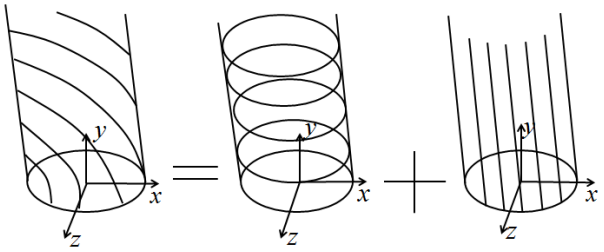

Figure 1: Composition of oblique spiral vortex column

Depending on the fixed vortex system model for a rotor with *k* blades, the circular rector of each blade was denoted by Γ that remains unchanged along the radius. Regarding a central angle $d\theta$ corresponding to an infinitesimal element bound vortex of the slant cylindrical vortex surface, its circular rector was represented by $\frac{k\Gamma}{2\pi}d\theta$. Moreover, $M(r,\psi)$ stands for a point in the disc.

With regards to the circular vortex cylinder, geometric meanings of various parameters are presented in Figure 2. To be specific, $\vec{l}$ refers to the distance from $\vec{ds}$ (a vortex line microsegment) to Point M, and ds_0 and l_0 to respective projections of vortex line microsegments $\vec{ds}$ and $\vec{l}$ on the disc. As for the straight vortex cylinder, its vortex line microsegment processing method is similar to that of the circular vortex cylinder.

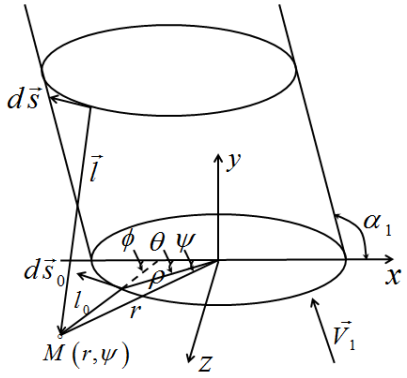

Figure 2: Calculation model of velocity induced by infinitesimal of ring vortex column

In a forward flight, circular rector Γ of a free vortex periodically changes in the direction of

azimuth angle. Here, it was expanded as Fourier series along this angle, taking its first-order value.

$$\Gamma = \Gamma_0 + \Gamma_{1c}\cos\theta + \Gamma_{1s}\sin\theta \tag{1}$$

Considering that the induced velocity varies periodically along the azimuth angle in a forward flight, the induced velocity was also expanded as Fourier series along the azimuth angle, taking its first-order value as well[4]:

$$v_y = v_0 + v_{1c}\cos\psi + v_{1s}\sin\psi \tag{2}$$

Where

$$v_0 = \frac{1}{2\pi}\int_0^{2\pi} v_y d\psi$$
$$v_{1c} = \frac{1}{\pi}\int_0^{2\pi} v_y \cos\psi d\psi$$
$$v_{1s} = \frac{1}{\pi}\int_0^{2\pi} v_y \sin\psi d\psi$$

Through integration based on the Biot-Savart Law[5] and a calculation model built according to Figure 2, the axial induced velocity of a single vortex cylinder relative to a point in the disc can be expressed as follows:

$$\begin{aligned}
\bar{v}_0 &= \bar{\Gamma}_0 \frac{k}{4\pi^2 \bar{V}_1} J_0 + \\
&\quad \bar{\Gamma}_{1c} \frac{k}{16\pi^3 \bar{V}_1}\left[\begin{array}{l}\dfrac{4\pi\cdot(\sec a_1 - \tan a_1)}{\bar{\rho}}\cdot \\ \left(\bar{l}\cdot E - \dfrac{\bar{r}^2+\bar{\rho}^2}{\bar{\rho}}F\right)\end{array}\right] + \\
&\quad \bar{\Gamma}_{1s} \frac{-k}{8\pi^3 \bar{V}_1} J_1 \\
\bar{v}_{1c} &= \bar{\Gamma}_0 \frac{k(1-\sin a_1)}{2\pi^2 \bar{r}\bar{V}_1 \cdot \cos a_1}\left[\bar{l}\cdot E - \frac{\bar{r}^2+\bar{\rho}^2}{\bar{l}}F\right] + \\
&\quad \bar{\Gamma}_{1c} \frac{k}{8\pi^3 \bar{V}_1} J_2 + \\
&\quad \bar{\Gamma}_{1s} \frac{k}{8\pi^3 \bar{V}_1}\left[\begin{array}{l}-\dfrac{2\pi\bar{V}_1}{\bar{r}\cdot\bar{\rho}}\left(\bar{l}\cdot E - \dfrac{\bar{r}^2+\bar{\rho}^2}{\bar{l}}F\right)\cdot \\ \sec a_1(\cos a_1 - 2\sec a_1 + 2\tan a_1)\end{array}\right] \\
\bar{v}_{1s} &= \bar{\Gamma}_0 \frac{k}{2\pi^2 \bar{r}} \frac{(1-\tan\frac{a_1}{2})}{(1-\tan\frac{a_1}{2})} J_3 + \\
&\quad \bar{\Gamma}_{1c} \frac{k}{8\pi^3 \bar{V}_1}\left[\begin{array}{l}-\dfrac{2\pi\bar{V}_1}{\bar{r}\cdot\bar{\rho}}\left(\bar{l}\cdot E - \dfrac{\bar{r}^2+\bar{\rho}^2}{\bar{l}}F\right)\cdot \\ \sec a_1(\cos a_1 - 2\sec a_1 + 2\tan a_1)\end{array}\right] + \\
&\quad \bar{\Gamma}_{1s} \frac{k}{8\pi^3 \bar{V}_1} J_4
\end{aligned} \tag{3}$$

All variables in the above equation have been nondimensionalized[6], More particularly, F $\left(\frac{\pi}{2},K\right)$ and E$\left(\frac{\pi}{2},K\right)$ respectively represent complete elliptic integral of the first and the second kind, which can be figured out by means of programming with MATLAB. Meanings of remaining variables are as follows:

$$K=\sqrt{\frac{4\bar{r}\,\bar{\rho}}{(\bar{r}+\bar{\rho})^2}}$$

$$\bar{l}=\bar{r}+\bar{\rho}$$

$$J_0=\begin{cases}0 & \bar{r}>\bar{\rho}\\ -\pi & \bar{r}<\bar{\rho}\\ -\dfrac{\pi}{2} & \bar{r}=\bar{\rho}\end{cases}$$

$$J_1=\begin{cases}0 & \bar{r}>\bar{\rho}\\ -\dfrac{2\pi^2\bar{V}_1(\cos\frac{a_1}{2}-\sin\frac{a_1}{2})}{\bar{\rho}(\cos\frac{a_1}{2}+\sin\frac{a_1}{2})} & \bar{r}\le\bar{\rho}\end{cases}$$

$$J_2=\begin{cases}\dfrac{2\pi^2\bar{\rho}\sin a_1}{\bar{r}+\bar{r}\sin a_1} & \bar{r}>\bar{\rho}\\ -\dfrac{2\pi^2\bar{r}\,\bar{\rho}\sin a_1}{\bar{\rho}+\bar{\rho}\sin a_1} & \bar{r}<\bar{\rho}\end{cases}$$

$$J_3=\begin{cases}\pi & \bar{r}>\bar{\rho}\\ 0 & \bar{r}<\bar{\rho}\end{cases}$$

$$J_4=\begin{cases}\dfrac{2\pi^2\bar{\rho}}{\bar{r}+\bar{r}\sin a_1} & \bar{r}>\bar{\rho}\\ -\dfrac{2\pi^2\bar{r}}{\bar{\rho}+\bar{\rho}\sin a_1} & \bar{r}<\bar{\rho}\end{cases}$$

For an actual flow, circular rector of the free vortex changes in the radial direction of blade. For simplification of relevant calculations, an infinite number of slant vortex cylinders were discretely classified into 5 slant concentric vortex cylinders[7-8]. Escapement points and circular rector intensity of such five vortex cylinders are illustrated in Figure 3. Moreover, the induced velocity at a point in the disc is generated because of the induction by these slant concentric vortex cylinders.

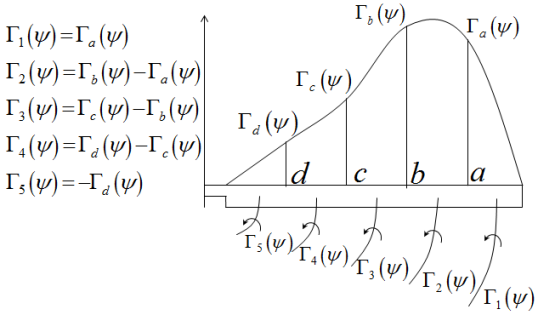

Figure 3: Diagram of escaped position and circulation strength of the dispersed vortex column

In a forward flight, circular rector of the blade bound vortex also changes along the azimuth angle. Likewise, it was also expanded as the Fourier series based on the corresponding azimuth angle, taking its first-order value as well.

$$\bar{\Gamma}_{bound} = \bar{\Gamma}_{bound0} + \bar{\Gamma}_{bound1c}\cos\theta + \bar{\Gamma}_{bound1s}\sin\theta \tag{4}$$

According to the blade element theory, the Kutta-Joukowski theorem and the motion equation of flapping, harmonic coefficients at various orders can be expressed as follows as far as the circular rector of the bound vortex is concerned:

$$\begin{aligned}
\bar{\Gamma}_{bound0} &= \frac{1}{2}a_\infty \bar{b}\left[\theta_0\bar{\rho} + \Delta\phi\bar{\rho}^2 + \frac{1}{2}\theta_2 u + \lambda_0 - \bar{v}_0(\bar{\rho}) + \frac{1}{2}a_1\mu\right] \\
\bar{\Gamma}_{bound1c} &= \frac{1}{2}a_\infty \bar{b}\left[\theta_1\bar{\rho} - \bar{v}_{1c}(\bar{\rho}) - a_0 u + b_1\bar{\rho}\right] \\
\bar{\Gamma}_{bound1s} &= \frac{1}{2}a_\infty \bar{b}\left[\theta_0 u + \Delta\phi\bar{\rho}u + \theta_2\bar{\rho} - \bar{v}_{1s}(\bar{\rho}) - a_1\bar{\rho}\right]
\end{aligned} \tag{5}$$

In this paper, the circular rector is represented by the Fourier series. Regarding the bound and the free vortices, their harmonic coefficients at various orders are equivalent to each other accordingly. In combination with Equation (5) expressing the blade bound vortex, the following formula was obtained (with items associated with the torsion angle and the flapping coefficient excluded):

$$\begin{cases}
\bar{\Gamma}_{10}(\psi) = \frac{1}{2}a_\infty \bar{b}\left[\theta_0\bar{\rho}_a + \lambda_0 - \bar{v}_0(\bar{\rho}_a)\right] \\
\bar{\Gamma}_{11c}(\psi) = \frac{1}{2}a_\infty \bar{b}\left[-\bar{v}_{1c}(\bar{\rho}_a)\right] \\
\bar{\Gamma}_{11s}(\psi) = \frac{1}{2}a_\infty \bar{b}\left[\theta_0 u - \bar{v}_{1s}(\bar{\rho}_a)\right] \\
\bar{\Gamma}_{20}(\psi) = \frac{1}{2}a_\infty \bar{b}\left[\theta_0(\bar{\rho}_b - \bar{\rho}_a) + \bar{v}_0(\bar{\rho}_a) - \bar{v}_0(\bar{\rho}_b)\right] \\
\bar{\Gamma}_{21c}(\psi) = \frac{1}{2}a_\infty \bar{b}\left[\bar{v}_{1c}(\bar{\rho}_b) - \bar{v}_{1c}(\bar{\rho}_a)\right] \\
\Gamma_{21s}(\psi) = \frac{1}{2}a_\infty \bar{b}\left[\bar{v}_{1s}(\bar{\rho}_b) - \bar{v}_{1s}(\bar{\rho}_a)\right] \\
\vdots \\
\vdots
\end{cases} \tag{6}$$

In the above formula, harmonic coefficients at various orders of the induced velocity are expressed in Equation (3). Through arrangement of Equation (6), a system of linear equations is obtained for harmonic coefficients at various orders of the free vortex's circular rector:

$$\boldsymbol{A}_{15\times15}\bar{\boldsymbol{\Gamma}}_{15\times1} = \boldsymbol{B}_{15\times1} \tag{7}$$

Where, $\bar{\boldsymbol{\Gamma}}_{15\times1} = \left[\bar{\Gamma}_{10}, \bar{\Gamma}_{11c}, \bar{\Gamma}_{11s}, \bar{\Gamma}_{20}, \bar{\Gamma}_{21c}, \bar{\Gamma}_{21s}\ldots\right]^T$,Considering that all slant cylinders are concentric cylindrical vortex surfaces, included angles, denoted as a_1, between each of the 5 free vortex cylinders and the axis-x are equal mutually. According to the corresponding definition, we have:

$$a_1 = \arctan\frac{\lambda_0 + \bar{v}_{dx}}{\mu} \tag{8}$$

The resultant velocity of the relative wind is:

$$\bar{V}_1 = \sqrt{\mu^2 + (\lambda_0 + \bar{v}_{dx})^2} \tag{9}$$

Where, $\bar{v}_{dx}$ refers to the equivalent induced velocity of the disc[9-11]. It is a constant in the direction of the radius and can be defined as follows:

$$\bar{v}_{dx} = \int_0^1 \bar{v}_0 \bar{r} d\bar{r} \Big/ \int_0^1 \bar{r} d\bar{r} \tag{10}$$

As defined above, it is clear that 5 slant free vortex cylinders have equal resultant velocities of relative wind.

Regarding the specific solving process, it is described below:

Step 1: Basic parameters of the rotor should be preseted, including radius R of the blade and its installation angle θ_0; and the forward speed V_0 and the initial equivalent induced velocity $\bar{v}_{dx}$ should be preseted to calculate the resultant velocity $\bar{V}_1$ of the air flow;

Step 2: We should solve the system of linear equations $\boldsymbol{A}_{15\times15}\bar{\boldsymbol{\Gamma}}_{15\times1} = \boldsymbol{B}_{15\times1}$, thus acquiring harmonic coefficients at various orders for 5 free vortex cylinders;

Step 3: We could substitute harmonic coefficients at various orders obtained for the circular rector of the free vortex into the expression of induced velocity, and calculate harmonic coefficients at various orders for the induced velocity in the disc;

Step 4: According to the induced velocity acquired, we calculate the result velocity $\bar{V}_1'$ of air flow in the disc;

Step 5: We should compare $\bar{V}_1'$ acquired in the above step with its initial value to judge whether it converges or not according to a convergence criterion of $\left|\bar{V}_1 - \bar{V}_1'\right| \le 10^{-6}$. If convergence can be confirmed, harmonic coefficients at various orders should be outputted for the circular rector of free vortices and the induced velocity in the disc; otherwise, $\bar{V}_1'$ figured out needs to be substituted into the equation and Steps 2-4 be repeated up until a convergence solution is obtained.

3. Analyses on aerodynamic characteristics of the autorotating rotor

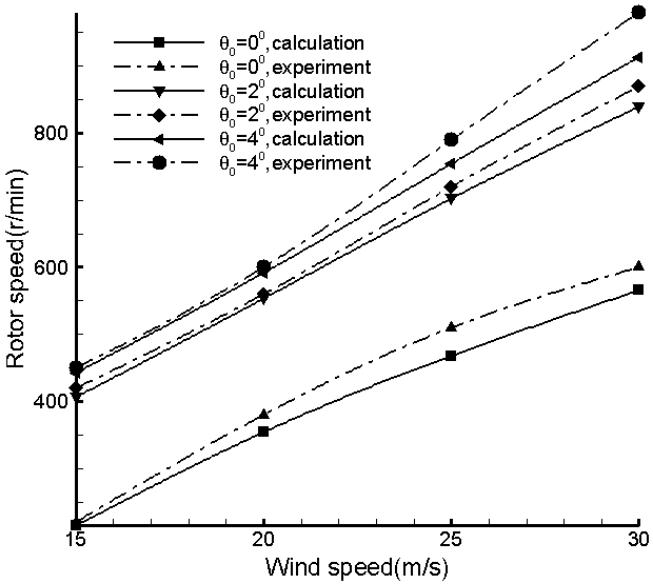

Figure 4: Stable rotating speed changes with relative flow

By virtue of the above method, a rotor model raised in Literature [12-13] was selected to calculate and analyze its aerodynamic characteristics. Parameters of this rotor are as follows: (1) Airfoil:

ONERA OA212; (2) number of blades: 2; (3) radius: 1.25 m; (4) hub radius: 0.25 m; (5) chord length: 0.095 m; (6) back chamfer angle a_s of propeller shaft: $4°$; and(7) installation angle θ_0 of the blade: $0°$, $2°$ and $4°$, respectively. Regarding the wind velocity V_0, it was set as $15m/s$, $20m/s$, $25m/s$ and $30m/s$. In this case, c_l and c_d in a condition of different values of the Reynolds number were inputted into the program by means of fitting to figure out stable rotating speed and lift of the autorotating rotor:

As can be observed from Figures 4 and 5, both the stable rotating speed and the life of an autorotating rotor increase as the wind velocity is raised. In addition, they are also in direct proportion to the blade installation angle. If the forward flight speed is further elevated, the lift goes up substantially in spite of insignificant variations of the stable rotating speed. Calculated values of stable rotating speed and lift of the autorotating rotor are basically consistent with corresponding experimental data, which proves that this model is valid and also satisfies engineering application requirements.

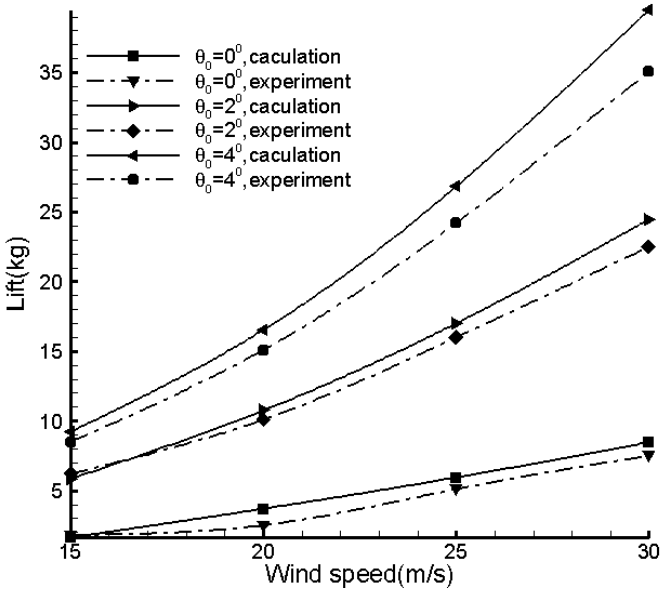

Figure 5: Lift changes with relative flow

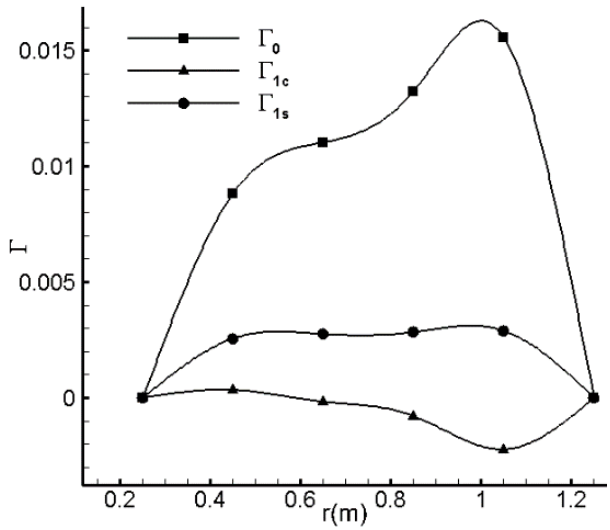

Figure 6: Harmonic coefficient of attached vortex circulation changes along the paddle

Specific to the above blade, we figured out distribution of harmonic coefficient at various orders, in a radial direction of the blade, for the induced velocity and the circular rector of the blade bound vortex provided that the forward flight velocity V_0 was selected to be $30m/s$, the back chamfer angle a_s of propeller shaft to be $4°$ and the installation angle θ_0 of the blade to be $2°$, as depicted in Figures 6 and 7. In these figures, both the circular rector and the induced velocity have been nondimensionalized.

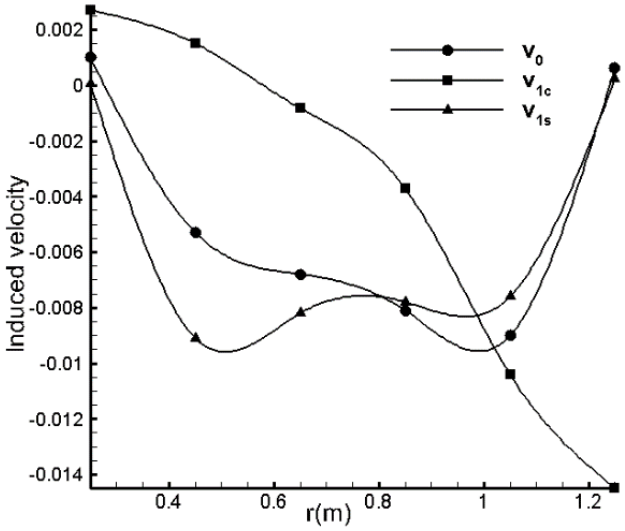

Figure 7: Harmonic coefficient of induced velocity changes along the paddle

Figure 6 presents how harmonic coefficients at various orders of the blade bound vortex circular rector vary along the blade. Concerning circular rectors of the bound vortex, the zero-order item $\bar{\Gamma}_0$ plays a leading role and reaches its peak around $0.7R$ (the circular rector). Regarding $\bar{\Gamma}_{1c}$ and $\bar{\Gamma}_{1s}$, their values are rather small, showing slight changes in a radial direction. This indicates that circular rector of the bound vortex changes insignificantly along the azimuth angle, but changes dramatically in the radial direction of the blade.

Figure 7 illustrates how harmonic coefficients at various orders of the induced velocity change along the blade. As can be seen, induced velocity variations in the disc are rather complex; and radial variations in harmonic coefficients at various orders are not exactly the same. In the entire disc, induced velocities are distributed in a nonuniform way. Therefore, induced velocity distribution processing may incur large errors on the premise of assuming such velocities to be distributed uniformly or linearly in the radial direction of the blade.

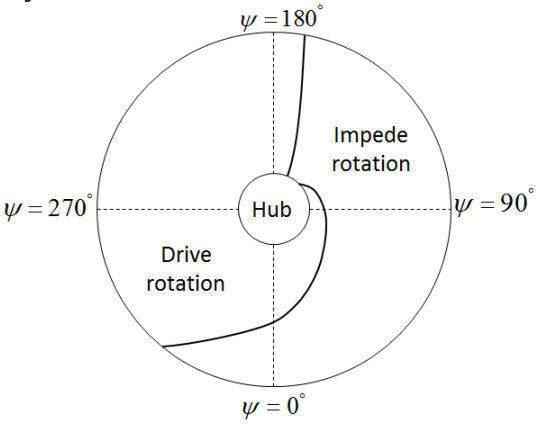

Figure 8: Distribution of driven rotating region and hindering rotating region in the disc

In Figure 8, torques in the disc in a forward flight are in asymmetric distribution; and the driving region falling into the retreating side can be larger. In this case, the resisting region falls on the advancing side. In a condition of steady autorotation, a sum total of torques achieved for driving and resisting regions is 0. Therefore, no reverse torque is transferred to fuselage when the autogiro is in a steady flight, in which case, no tail rotor is needed to maintain the balance of fuselage.

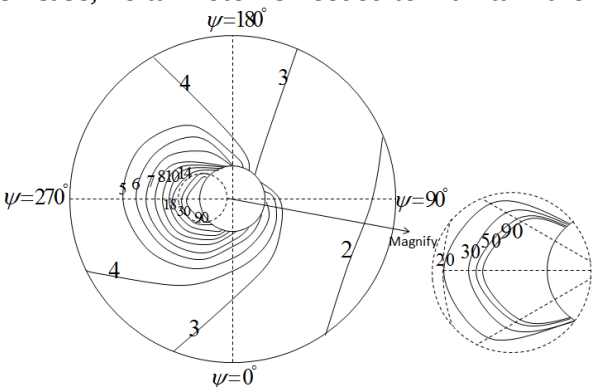

Figure 9: Distribution of attack in the disc

Incidence distribution in the disc is plotted in Figure 9. Clearly, incidences in the disc are asymmetrically distributed in a forward flight. When different section shapes of the same blade are in operation subjecting to diverse incidences, different azimuth angles correspond to different incidences even on the same section shape. In other words, section shape incidences change periodically during autorotation for the following reasons. Under the circumstance that forward speed projection on the disc changes as the azimuth angle varies, wind velocity of advancing blade is not equal to that of the retreating blade on one hand; and on the other hand, distribution of induced velocities is nonuniform. Consequently, incidences are distributed asymmetrically.

According to Figure 9, section shape incidences of the retreating blade are larger than those of the advancing blade at the same radial position; and a high incidence region is mainly formed nearby the blade root forming an angle of $270°$ with the retreating blade. If the selected airfoil stalls when the incidence is $14°$ and above, a stall region takes form near the blade root with an azimuth angle of $270°$; and in the stall region, a high incidence greater than $90°$ is formed. Therefore, the presence of a reversed flow region is proved.

4. Conclusion

(1) By improving the blade element theory, aerodynamic characteristics of the autorotating rotor are analyzed in this study. Comparing with the conventional version, the improved blade element theory has some main advantages. Thanks to the fixed wake approach selected for an infinite number of blades, distribution of the induced velocities in the disc is obtained; and in combination with the blade element theory, aerodynamic characteristics can be analyzed for the autorotating rotor. Calculated values of stable rotating speed and lift of the autorotating rotor are found to basically conform to their experimental data, proving validity of the proposed model. Induced velocity expressions obtained based on the fixed wake approach have explicit physical meanings. Relevant practice shows that iterative operation of the circular rector and the induced velocity converges rapidly, which spares computing time and has certain engineering application values for analyzing aerodynamic characteristics of the autorotating rotor.

(2) In a forward flight, torques at the disc are in asymmetric distribution, making resisting region falling on the advancing blade larger. As regards a helicopter[14], its rotor is driven by the engine and thus rotates, so that resisting torque in the entire disc needs to be above the driving torque. In this

scenario, the corresponding reverse torque enables the fuselage to rotate and thus a tail rotor is needed to maintain the balance of fuselage. Comparatively, a stable flight of an autorotating rotor is on the premise of making resisting torque on the entire disc equal to driving torque. Therefore, no reverse torque is transferred to the fuselage during the flight and no tail rotor is required for the purpose of maintaining fuselage balance.

(3) Section shape incidence of the retreating blade in a forward flight is larger than that of the advancing blade at the same radial position. Concerning the helicopter[15], its high incidence is at the retreating blade tip; however, the high incidence of an autorotating rotor is at the root. For a reason that the blade root region has a minor influence on rotor lift and incidences at middle and tip sections of the rotor blade are rather low, it is much less likely for the entire rotor to stall. By contrast to helicopters, therefore, autogyro performs better in safety.

References

[1] Zhu Q H. Reseach on key technologies of gyroplane preliminary design [D], Nanjing university of Aeronautics and Astronautics, 2007.

[2] Wang P, Wang S C, Guo C G. Rigid-Wake Analysis of Coaxial Rotor in Hover Aerodynamics[J]. Journal of Nanjing university of Aeronautics and Astronautics, 1997, 29(6):708-710.

[3] Wang S C. Helicopter Aerodynamics [M]. Nanjing university of Aeronautics and Astronautics Press, 1993.

[4] Wang S C. Some doubts in helicopter aerodynamics [J]. Nanjing: Journal of Nanjing university of Aeronautics and Astronautics, 2003, 3(35):225-230.

[5] Chen M, Hu J Z. A method of spatial distribution of helicopter rotor induced velocity [J]. Acta Aerodynamica Sinica. 2005, 23(3):339-349.

[6] Zhu Q H, Li J B, Ni X P, et al. Study on aerodynamic characteristics of autorotating rotor and jump takeoff performance of gyroplane[J]. Acta Aerodynamica Sinica. 2008, 26(3):282-286.

[7] Wang H J, Gao Z. Aerodynamic virtue and steady rotary speed of autorotating rotor [J]. Avta Aero nauticaet Astronautica Sinica, 2001, 22(4):337-339.

[8] Wang J C, Tan J F, Li J B, et al. Investigation of autorotating rotor aerodynamic characteristics based on free wake method[J]. Acta Aeronauticset Astronautics Sinica, 2015, 36(11):3540-3548.

[9] Ji L Q, Zhu Q H, Cui Z, et al. Research on aero-Dynamic characteristics of autorotating coaxial twin- rotor[J]. Journal of Aerospace power, 2012, 27(9):2013-2020.

[10] Wei J B, Xue X Z, Shu J R. An Iterative Solution to the Rotor Attachment Vortex Circulation Distribution [J]. Journal of Ballistics, 2003, 15(1):60-63.

[11] Liu P Q. Air Propeller Theory and Applications [M]. Beijing University of Aeronautics and Astronautics Press, 2005.

[12] Wang H J, Gao Z. Experiment research on the rotor autorotation state for a high-speed helicopter scheme [J]. Avta Acta Aerodynamica Sinica Sinica, 2004, 22(2):151-155.

[13] J. Gordon Leishman. Development of the Autogyro: a Technical Perspective [J]. Journal of Aircraft, 2004, 41(4):765-781.

[14] Ji L Q, Zhu Q H, Li J B. Experimental investigation on aerodynamic characteri- stics of autorotating coaxial twin-rotor and single rotor[J]. Journal of Experiments in Fluid Mechanics, 2013, 27(5):7-10.

[15] Xia L, Liu H. Helicopter Rotor Autorotation Landing Safety Research [J]. Helicopter Technique, 2005, 143(3):15-17.